energies

MDPI

Article

Profiling Corrosion Rates for Offshore Wind Turbines with Depth in the North Sea

Waseem Khodabux [1,*], Paul Causon [1] and Feargal Brennan [2,*]

[1] School of Water, Energy and the Environment, Renewable Energy Marine Structures—Centre for Doctoral Training (REMS-CDT), Cranfield University, Bedfordshire MK43 0AL, UK; p.causon@cranfield.ac.uk
[2] Department of Naval Architecture, Ocean & Marine Engineering, University of Strathclyde, Glasgow G4 0LZ, UK
* Correspondence: m.w.khodabux@cranfield.ac.uk (W.K.); feargal.brennan@strath.ac.uk (F.B.)

Received: 6 April 2020; Accepted: 8 May 2020; Published: 15 May 2020

Abstract: Corrosion in the marine environment is a complex and expensive form of damage. It is commonly studied by the deployment of coupons that reflect the marine corrosion a structure will experience, thus allowing design and maintenance prevention strategies to be developed accordingly. This study stems from the lack of information in the literature regarding the profiling of corrosion with respect to marine depth in the North Sea where important wind farm developments have been undertaken. To address such issue a field experiment has been designed and carried out in the vicinity of the Westermost Rough Windfarm in the North Sea. The field experiment consists of deploying steel S355 coupons below the tidal area and capturing the effects of corrosion, the mass loss from which the corrosion rate is derived and the chemical products that makes up the rust with water depth. The study involves proper planning and logistics to ensure that the field experiment survives the rough conditions of the North Sea for a duration of 111 days. A high corrosion rate of 0.83 mm/year has been observed in this experiment. This paper goes into the details of the deployment blueprint employed and the analyses of the coupons to provide a conclusive observation and modelling of corrosion with respect to water depth under free or open sea water corrosion condition.

Keywords: North Sea; mass loss; chemical analysis; corrosion rate; sea depth

1. Introduction

Marine corrosion is a complex process, especially for steel structures. There are various interactions between the metal matrix and the marine environment which alter the corrosion. This interaction is affected by several factors such as the temperature, dissolved oxygen, pH and salinity being flagged as the most important ones.

The temperature of the oceans has changed significantly over the years due to global warming and its effect in such a complex environment requires tracking and comparison. The metals used for structural purposes for ships, offshore wind turbines (OWT), and oil and gas platforms have evolved substantially in terms of the strength of the materials. Their corrosion resistance needs to be assessed accordingly.

The OWT will undoubtedly suffer from corrosion if left unprotected [1]. The designers have borne this in mind and have been careful in the strategy for the corroding piles by including different corrosion protections especially in the immersed sections and splash zones of the monopile where in general it is considered to be highly influenced by corrosion [2–7].

If left unprotected, the structures are very likely to suffer from a myriad of corrosion mechanisms. Often, OWT tend to be compared to oil and gas platforms. Despite some similarities and standards being inspired from the oil and gas practices, there are some fundamental differences, particularly in

the scope of accessibility and economics. The OWTs are all unmanned structures with highly restricted access [8]. Therefore, the maintenance strategy is more complicated and the evolution of corrosion in the structures can be rather difficult to gauge. Important paint failures have been observed on OWTs after only two years in service [9]. The costs of repair are generally elevated costing about 1000 Euro per m^2, which is about 50 times more than the initial coating cost. Those costs pile up and cause a hike in the levelised cost of energy (LCOE) [10]. The economic perspective is important and worth mentioning. An offshore wind farm will take 15 to 20 years to break even whereas an oil and gas platform will take up to seven years [11,12]. Expensive maintenance is, therefore, by no means a financial strain on the oil and gas platforms but takes a very different interpretation in the OWT portfolio.

The major problem with respect to corrosion took the industry by surprise [13]. It was expected to be non-existent and the design standards took a relaxed approach on this aspect [14]. It is related to the corrosion of the inner section of the monopiles [14]. To make more sense, it is crucial to understand the design of the monopiles and the connection of the various sections, like the transition piece (TP), platforms and decks.

The monopile is a steel pile driven into the seabed that surpasses the sea surface by one to two metres. The transition piece (TP) is slotted on to the top of this free section with an overlap of about six metres. Brackets are used inside the monopile to orient the TP. The empty spaces left are then filled in with high strength grout that bond the two sections together. There are two other platforms that are then connected. The first one being the service platform located between the monopile and the TP and the airtight deck or platform that seals and secludes the upper section of the turbine from the lower one. The airtight platform usually has an opening which allows the J-tube to go through and exit the monopile in the seabed region through another opening at this section of the monopile [15].

There have been reports of a considerable amount of grout failure in European wind energy projects. In addition to changing the load patterns and increased fatigue damage, there have been seawater leakages that have initiated corrosion sites. It should be highlighted that corrosion at those regions were unexpected [15].

The fully sealed compartments have not been achieved and these have been revealed in the most severe form upon routine inspection. A survey was set up in one of the wind farms and it was observed that only 8% of the wind farms were corrosion free closed compartment. Of which, 70% had water exchanges with oxygen levels being above 15% and the remaining showed intermediate levels of oxygen transport. The seals and the airtight platform leakages were the main sites of oxygen ingress [15].

The water exchange has resulted in an internal environment that promotes corrosion and is highly dependent on the tides. Water levels rise and fall with the tide inside the column as they do outside [13], which creates wetted and immersed areas.

Corrosion in an OWT has been observed at different locations and it has to be specified that there are various corrosion mechanisms existing. Different regions affected by corrosion can be broken down as listed below and further illustrated in thriving shown in Figure 1a,b [16–18]:

- Atmospheric zone
- Splash zone
- Submerged zone
- Mud zone

In a sealed structure, the dissolved oxygen is rapidly absorbed and the medium becomes anaerobic causing hydrogen sulphide to be released as a product of the new corrosion mechanism. Within a closed environment it is expected that this form of corrosion would be limited as the internal conditions would not continue to support the chemical reaction [15].

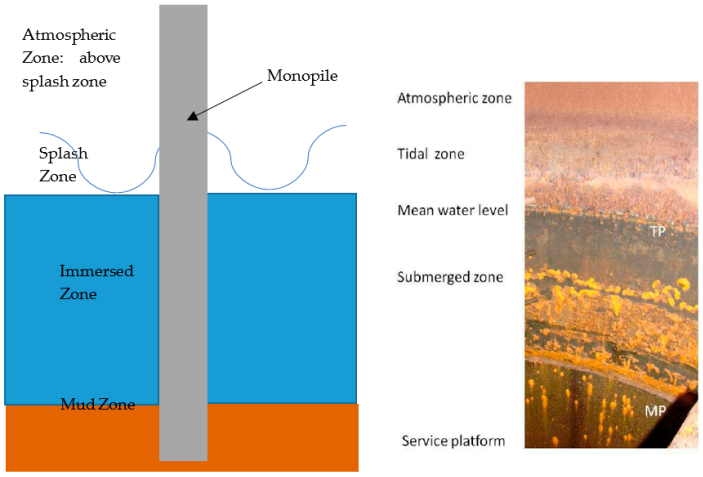

Figure 1. (**a**) different corrosion levels inside the monopole. (**b**) corroded regions inside monopiles [13].

In reality though, partial oxygenation affects corrosion by promoting a more acidic environment and recently pits have been discovered [15]. Corrosion discovered for an OWT was of the following nature [13]:

- Mud zone: Differential aeration, microbial-induced corrosion (MIC) and hydrogen induced stress cracking (HISC)
- Waterline: pitting corrosion due to differential aeration
- Stagnant water causing important environmental discrepancies
- Weld defects causing corrosion fatigue and stress corrosion cracking (SCC)
- Acidification if sacrificial anodes are installed
- Accumulation of gases such as H_2S, H_2 and CH_4

Studies have been done in various parts of the world to capture the effects of marine corrosion on carbon steel. These variations have been observed by several authors but there seems to be absence of this effect with respect to the depth especially in the North Sea and for carbon steel. This study looks at the corrosion loss of carbon steel S355 used in the industry. A novel mooring approach capable of supporting multiple experiments simultaneously was designed and experimented; in this case a corrosion experiment with a marine growth (the colonisation of hard surfaces such as those provided by wind turbine substructures by marine organisms) experiment. The latter of which would not be discussed further beyond the description of shared structural elements. For example, the frames inside which corrosion coupons were mounted also functioned as a sampling structure for marine growth. The frames were made of either plastic (PVC) or S355 steel coated with interzone 954 anti-corrosion coating.

After 111 days of exposure further analyses have been done after cleaning the corrosion coupon. The first analysis being visual inspection and the mass loss and corrosion rates. From the corrosion product further information on corrosion rate with respect to depth can be deduced from the Energy Dissipative Spectra (EDS) analyser connected to the Scanning Electron Microscope (SEM). To characterise the chemical structure of the rust, the X-ray Diffraction method (XRD) has been used. It is to be noted that in the scope of this study biofouling and erosion have not been monitored.

2. Field Experiment Design and Deployment

Marine corrosion is complex and to understand the corrosion interaction as realistically between the metal and the environment, a field experiment has to be done. Marine field experiments can be considered to exist in three categories namely harbour or port, shallow and deep water. The port or harbour has a different environment with particularly high levels of pollutants. Accelerated low water

corrosion (ALWC) is usually experienced in those waters which is an aggressive form of microbial influenced corrosion (MIC) that may occur on steel in estuarine and marine structures [19,20]. ALWC has been observed to be enhanced with dissolved inorganic nitrogen (DIN) [21]. In general, coupons are suspended from fixed structure or the piles are removed after a number of years of service to capture the corrosion rate. The piles are able to capture the different regions (atmospheric, tidal, immersed, mudline and below the mudline) corrosion levels. This provides a full profiling which also provides the opportunity to characterise the corrosion mechanisms [22,23].

Deep water corrosion experiments are more challenging to perform. They require robust equipment that will sustain the high pressures [24]. As the offshore oil and gas exploration is moving further offshore, understanding the interaction between the environment and the metal at this depth is important. Coupons have been placed at depth of more than 1000 m for corrosion analysis [25]. Experiments have been done at a number of locations with varying results. Those experiments were done using a submerged buoy which is attached to coupons across different depths. An anchor is used as mooring and it is worth noting that this arrangement is used only in the immersed region [24].

For shallow water, coupons are often suspended from fixed structures like offshore oil and gas platforms, OWTs or offshore meteorological masts. The question for shallow waters is how to test for corrosion in an unexploited site. There have been many experiments done but none in the literature takes a detailed approach in profiling corrosion loss with depth in the past decade from the literature [26,27]. This will require a new design to accommodate the experiment to profile the corrosion rate and loss with depth and is explained below.

The entire experiment in shallow water of maximum water depth of 30 m consisted of five arrays, each comprising four coupons suspended inside a frame. The whole set-up was moored to the seabed by 250 kg gravity anchors made from two 125 kg webbed tubes tied together as shown in Figure 2a. In adverse weather conditions, the North Sea can be rough, with wave heights (from crests to troughs) of >10 m. The force generated by those waves was immense and would carry or displace large objects on the surface without any difficulty. Whilst completely avoiding large waves would not be achievable given the vertical depth profile of the mooring system, it was decided that a subsurface buoy, submerged below the minimum tidal height, would mitigate the effects in most weather conditions. As an air-filled buoy would suffer from compression effects caused by water pressure as the tide rises and falls, which could cause the buoy to become negatively buoyant and sink to the seabed at high tide, a foam-filled buoy was selected. A buoy which provided 90 kg buoyancy force was selected. It is of note that in using such an arrangement, the data could not be collected from the splash zone.

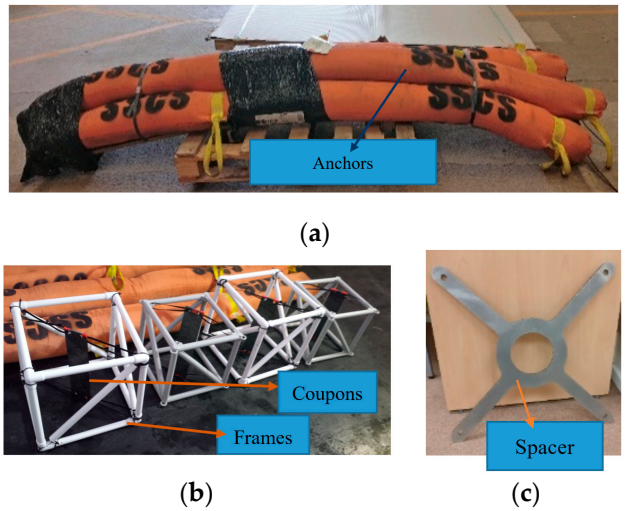

Figure 2. (**a**) Anchors that are attached to the frames, (**b**) Coupons mounted inside frames using high strength marine cable ties, (**c**) Line spacer that prevents twisting of the ropes.

Between the topmost frame (closest to the sea surface) and the submerged buoy and the bottommost frame and the anchor a device known as a line spacer was added. This device maintained the spread of the ropes, preventing them from twisting or compressing the array under tension.

The attachment of the plates to the frames varied depending on whether the frames were plastic or steel. For the steel frames, at each corner, a triangular bracket with a through hole of 10 mm diameter was drilled. The plates were connected to these attachment points using marine cable ties, which had a breaking strength of >150 kg. For the plastic frames, cable ties tightened around each corner formed the attachment points for the plates. The assembly of the plates and coupons are shown in Figure 1b.

Coupons

Carbon steel of S355 grade was used. Some experiments were carried in the past using coupons and the one most relevant in the literature was done in the North Sea for OWT corrosion monitoring having dimensions of $400 \times 90 \times 6$ mm^3 [1]. The same dimensions were used for this study. Four holes had been drilled into the coupon during manufacturing for attachment to the frame. It was kept to a minimal size as this region would have to be excluded in the study. The exposure time for the experiment covered 111 days.

Coupons were prepared to meet the ASTM G1 standards and were colour marked and numbered accordingly to depth. The depths chosen for deployment are shown in Table 1. The marine tape in the corners was used, as reference in case 3D cloud coordinate analysis would be done as shown in Figure 3. There was a potential problem that could arise from it. The water could flow beneath the layer of the tapes and introduce a limited amount of oxygen resulting in differential oxygen concentration causing crevice corrosion. As such, each of the spots where the tapes were applied were also glued on with extra strong marine glue, commonly used to patch holes in hulls of boats. The plates were colour coded based on which array they were to be deployed in, the plates code named as red, grey, black, blue and green. The front of each plate was denoted one to four strips of tape based on their relative position in their array (as shown in Figure 3): plate 1 (one strip at the top), plate 2 (two strips at the top), plate 3 (two strips at the top and one strip at the bottom), plate 4 (two strips at the top and two strips at the bottom). The corners of each plate were protected with a layer of tape to preserve a reference point for gauging the height of corrosion.

Table 1. Plate number with depth.

Plate Number	Height [m] (Distance from Seabed)
1	16
2	10.5
3	5.5
4	1

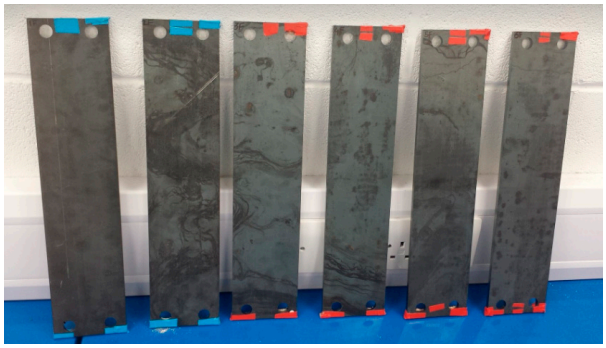

Figure 3. Colour coding and numbering of plates.

The mass of each plate was measured by a digital scale to an accuracy of 0.1 g. The results are displayed in the Appendix A.

2.1. Assembly

The assembly can be summarised in the charts shown in Figure 4a,b.

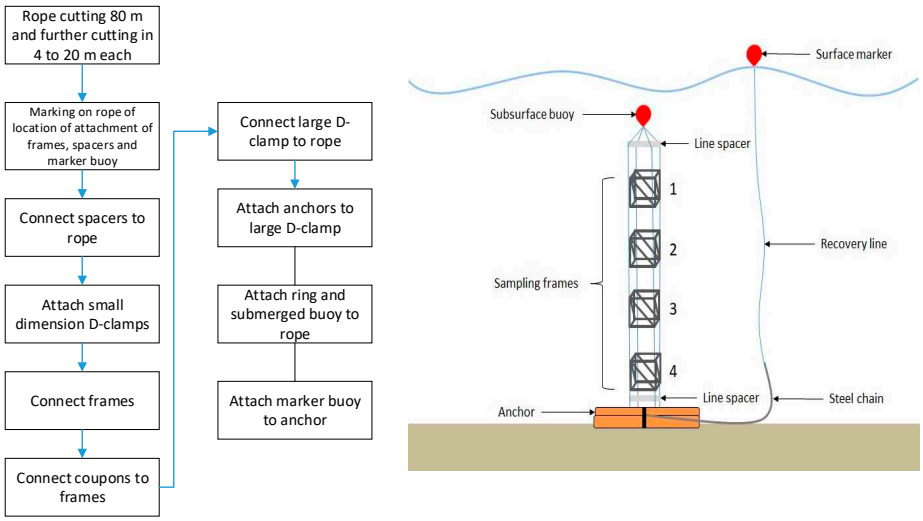

(**a**) (**b**)

Figure 4. (**a**) Array assembly up flowchart; (**b**) schematic of assembly.

2.2. Deployment and Recovery

Five arrays were deployed northwest of Westermost Rough Windfarm as shown in Figure 5. Array 1 was deployed several weeks ahead of arrays 2–4 to test the deployment method.

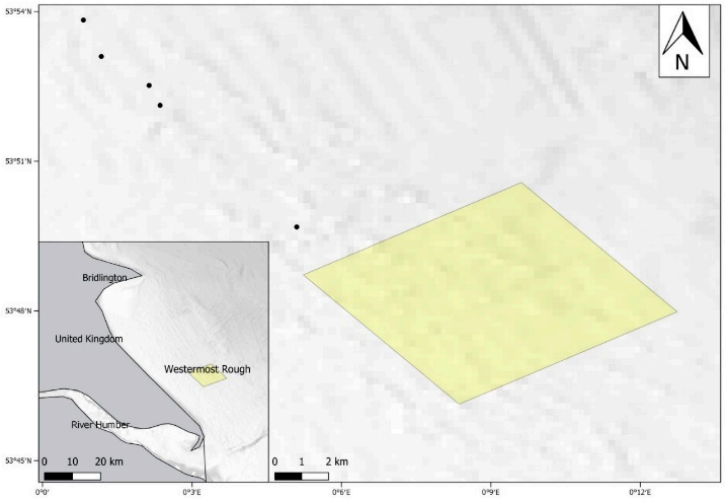

Figure 5. Map of array deployments (black points 1–5) relative to Westermost Rough offshore wind farm and Bridllington Harbour.

During deployment, a crane was used to lift the anchors over the stern of the vessel (Figure 6a). The frames were each lowered into the water (Figure 6b), starting with that closest to the anchor, followed by the mooring buoy (Figure 6c). Once the array was in the water the vessel was moved ahead to allow the array to straighten with the mooring buoy at the back. Finally, the surface marker buoy was dropped into the water and the anchors were released.

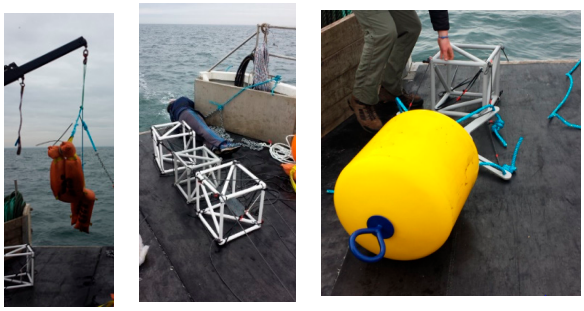

(**a**) (**b**) (**c**)

Figure 6. (**a**) Anchors going in, (**b**) Array going in water, (**c**) Submerged buoy being released in water.

The marker buoy remained on the surface to warn local vessel traffic of the hazard beneath the surface and for recovery at a later stage. It was planned that during recovery, the recovery line would be pulled aboard and connected to a winch. The anchor would then be winched up to the vessel, allowing the subsurface buoy to float to the surface along with the frames. However, the strength of the mooring ropes proved to be insufficient during the extreme weather and strong winds. Two of the arrays were recovered (Blue and Black) after the ropes failed and the moorings broke away from the anchor. The remaining arrays could not be re-located, but it can be assumed that they suffered a similar fate. For the arrays that were recovered, the steel frames had been damaged, but the corrosion coupons were still in place.

There is no way to determine when the mooring ropes failed, and the arrays broke away from the anchors. It was therefore assumed that the length of exposure, for the purposes of the analysis, would be from the deployment date to the collection date, which amounted to 111 days. In addition, the results would be displayed with respect to the depth (which is assumed as the exact depth of deployment and orientation cannot be fully traced due to the breaking effect), discussed more thoroughly from the observations, and compared to other experiments or industry standards mainly focussing on the seabed and submerged regions corrosion rate.

Since the profiling of the depth is unknown, the results section has been presented as a methodology to treat the corrosion data. The corrosion data obtained is then tested against other experiments from the literature in the discussion section to observe if there is a trend that can be established. The data reflects the depth profile of the marine corrosion as initially designed before the failure of the mooring ropes.

3. Results

After collection, the coupons were dried and photographed. Some of the residual material that had fallen off from each coupon was placed in a test tube for further chemical analysis.

The plates were cleaned according to the ASTM G1 standard where 1000 mL HCl, 20 g antimony trioxide (Sb_2O_3), 50 g stannous chloride ($SnCl_2$) were used and shown in Figure 7a,b [28].

(**a**) (**b**)

Figure 7. Samples: (**a**) before cleaning, (**b**) after cleaning.

3.1. Visual Inspection

The plates cleaned revealed high levels of corrosion and in some cases pitting corrosion was present shown in Figure 8a. In addition, the variation of the pits with respect to pit depth was noticeable and fell mainly in the small and shallow category to no visible pits represented in Figure 8b. An isolated case of crevice corrosion was found under the tape as shown in Figure 8c. At this stage, there were few broad pits, which tended to be formed by the mechanism of pit coalescence represented in Figure 9. Smaller pits were also present and when viewed under the magnifying glass provided a clear case that the new pits initiated on the plates were present and not noticeable with the naked eye. There seemed to be more than one could count just signifying that in 111 days, the presence of corrosion cannot be neglected or underestimated and localised corrosion is readily obvious.

(**a**) (**b**) (**c**)

Figure 8. (**a**) High levels of pitting; (**b**) Low levels of pitting; (**c**) Crevice corrosion under marine tape.

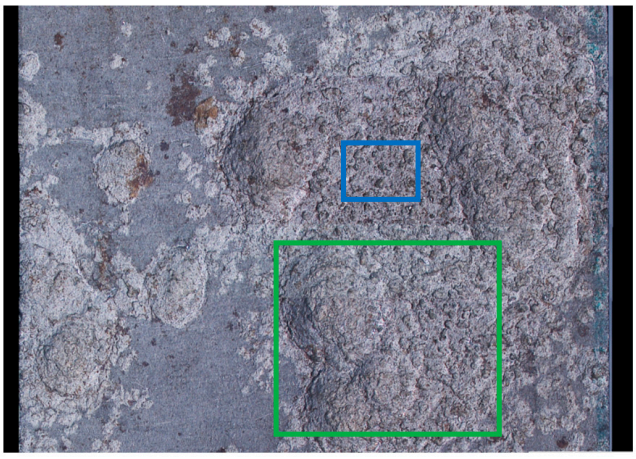

Figure 9. Pit coalescence highlighted in green and micro pits highlighted in blue.

Substantial variation was also observed between plates where the topological surfaces varied. More pitted regions accounted for a rougher surface compared to less pitted surface. It was also seen that in some cases on the same plate, some regions had important levels of pits whereas others did not, implying the nature of the pitting corrosion is highly localised on the plate for carbon steel.

It was estimated for instance in the 3-black case that the number of pits on the front side was more than that on its back side. This difference is hard to explain due to a variety of factors that have affected the experiment. This observation has to be re-tested though to come out of the hypothetical shell to a scientific explanation with appropriate instrumentation such as the water velocity, the corrosion current and the biological and chemical influences of the water combined together in the complex sea water without the failure of the ropes and the depth preserved. The surface was more rugged as shown by Figure 9 when pitting corrosion seemed to be the dominating form of corrosion.

3.2. Mass Loss and Corrosion Rate

The mass loss and corrosion rate are extremely important parameters those are generally used for design and monitoring of marine structures. They are assumed to be solely under the influence of uniform corrosion. This would give an insight of the harshness of the environment on the metal.

The raw data can be seen in Table A1 in the Appendix A section.

The mass loss was derived from the following equation:

$$\text{mass loss} = \text{original mass} - \text{final mass after acid cleaning} \tag{1}$$

The units measured were in grams.

Corrosion loss was derived from the mass loss and related to the density:

$$\text{Density} = \frac{\text{Mass loss}}{\text{Volume}} \tag{2}$$

The volume was that of a cuboid:

$$\text{Volume} = \text{Area X thickness loss} \tag{3}$$

The thickness loss could be calculated as:

$$\text{thickness loss} = \frac{\text{Mass loss}}{\text{Area X Density}} \tag{4}$$

The mass loss in 1-Black is more than 1-Blue by some margin as shown in Figure 10.

Figure 10. Mass loss (wt. %) of coupons due to corrosion, (before and after cleaning).

The number of days of exposure represented the thickness loss assumed to be uniform and from that principle the corrosion rate per year could be found:

$$\text{corrosion rate}\left[\frac{\text{mm}}{\text{year}}\right] = \frac{\text{thickness loss}}{\text{Number of exposure days}} \text{ X } 365.25\ . \tag{5}$$

Figure 11 show the results in terms of corrosion rate as a result of the mass loss.

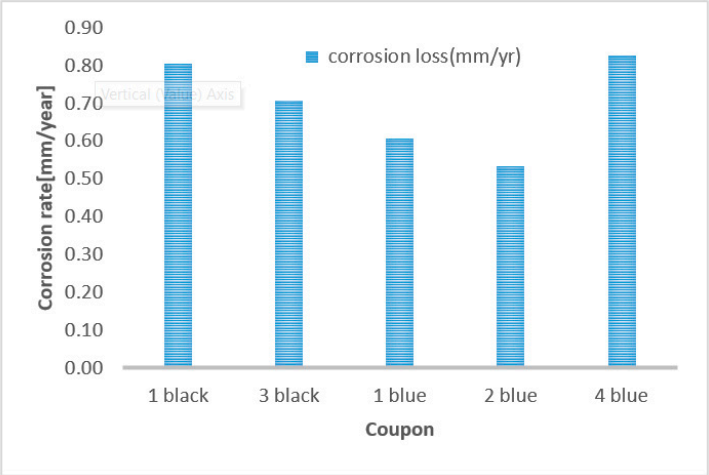

Figure 11. Variation of corrosion as a function of colour coded plate.

3.3. Chemical Analysis and Implications

This section was carried out as it could provide a deduction on the type of corrosion experienced by the metal. This required an analysis of the substrate through scanning electron microscope and the energy dispersive X-ray and the X-ray diffraction technique which will show how the elements combine together to form the rust product.

3.3.1. SEM and EDS

To be able to comprehend the variation, an assessment of the chemical products had been done which could be used to reflect the environmental conditions the plates were subjected to. The results for the EDS and the spectra can be found in Table A2 in Appendix B

The scanning electron microscopy (SEM) provides a view of the microstructure of the rust and the Energy Dispersive X-Ray Spectroscopy (EDS) provides the elements present in that specific region. Rust clusters were placed on the adhesive support that was later placed in SEM as demonstrated in Figures 12 and 13.

(**a**) (**b**)

Figure 12. (**a**) Rust sample on sample holders, (**b**) Sample in vacuum chamber for SEM analysis.

The results from the remaining clusters showed this similar behaviour and therefore it was concluded that iron and oxygen were the dominating products with important variations in the % composition of other elements.

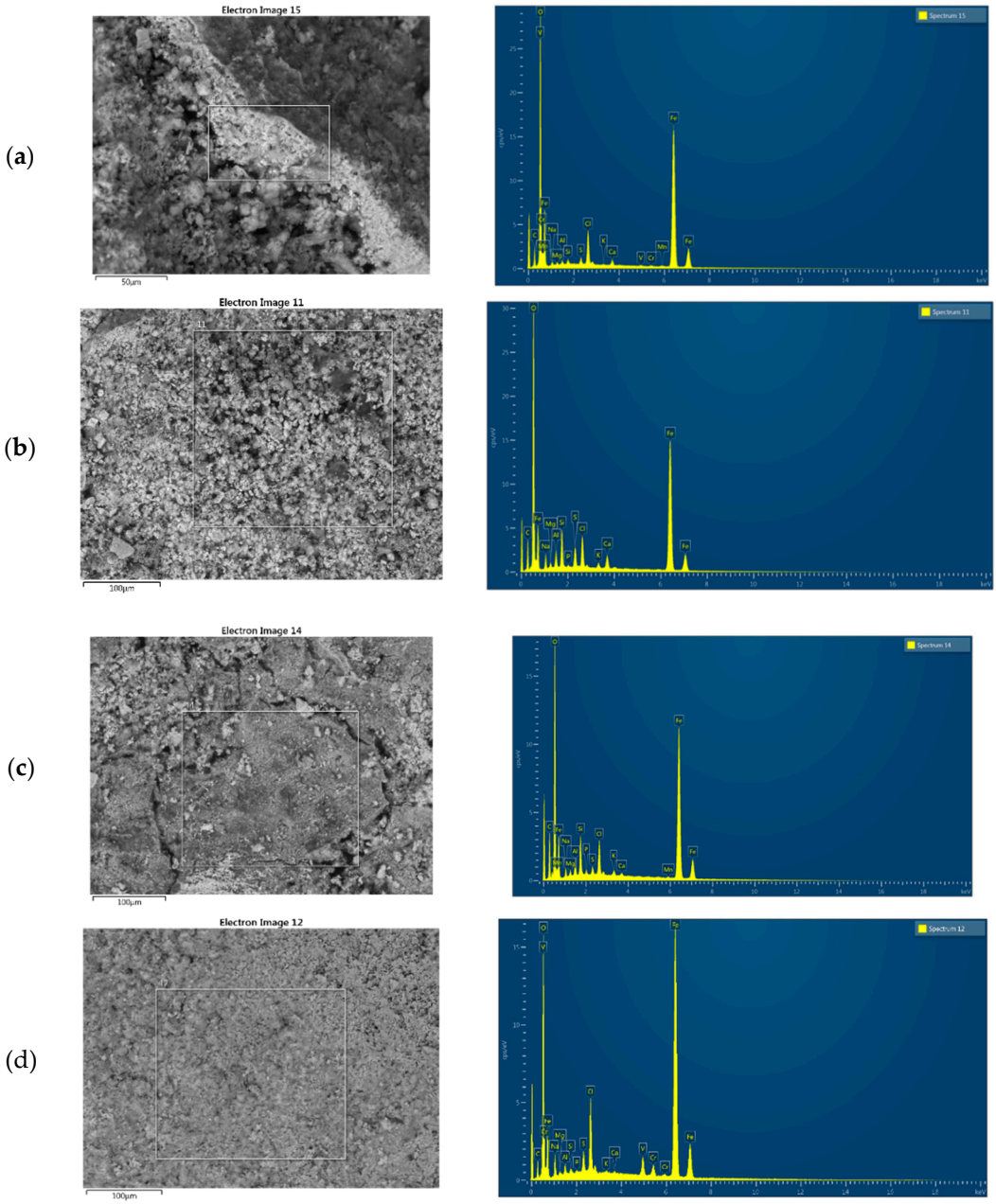

Figure 13. (**a**–**d**) Microscopic images of the rust samples (**a**–**d**) for EDS analysis.

3.3.2. XRD

The chemical products formed due to corrosion were determined using the XRD technique. The rust formed was iron oxide-hydroxide. The equipment is shown in Figure 14.

This suggested that the corrosion product was actually oxygen rich. No form of anaerobic corrosion was found due to the absence of sulphide-based products. Low sulphide content was observed in the plates after corrosion test from EDS analysis (Table 2).

XRD analysis of corrosion products can also give substantial information on the environmental condition of the sea compared to Pourbaix diagram of carbon steel. The product obtained falls in the passivation region of the Pourbaix diagram which can also explain the high region of pitting present.

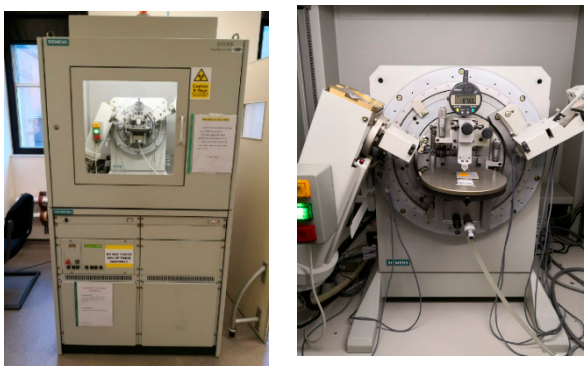

(**a**) (**b**)

Figure 14. (**a**–**b**) XRD equipment with rust sample being tested.

Table 2. Elemental composition (wt%) of corrosion product collected from colour coded plates.

Colour Coded Plate	%N	%S	%Cl	%Fe	Depth [m]
2 blue	0.00	0.79	2.90	46.86	10.5
2 black	0.00	0.34	1.86	52.55	10.5
4 blue	6.50	0.89	2.29	39.19	1
3 black	0.00	0.48	1.60	50.34	5.5
1 blue	0.00	1.09	2.53	38.67	16

4. Discussion

As a result of the trend of the mass loss with respect to depth and checking if the snapping of the rope had a major influence on the experiment with respect to depth, an investigative work was carried out with two objectives to charter out:

- The trend in corrosion with respect to depth
- The corrosion rate magnitude

A first point was covered mainly from a literature review. One article was isolated focussing on the immersed and sea bed corrosion and having the same arrangement as this study [29]. Comparing it would be challenging as the location and depth were dissimilar. Therefore, the depth and corrosion rate were normalised using the maximum normalisation method and plotted as shown in Figure 15

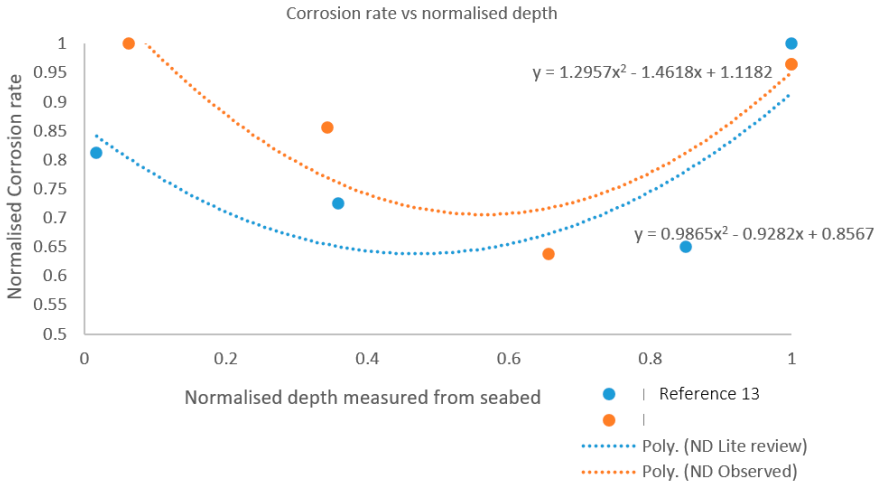

Figure 15. Comparison of literature review considering the normalized depth and corrosion rate.

It can be clearly seen that the general trends for both of them seem to have a trend dipping from the first data point to the third and then from the third to forth going upwards. This trend is synonymous of the quadratic function. The percentage error was found between the two curves is shown in Figure 16.

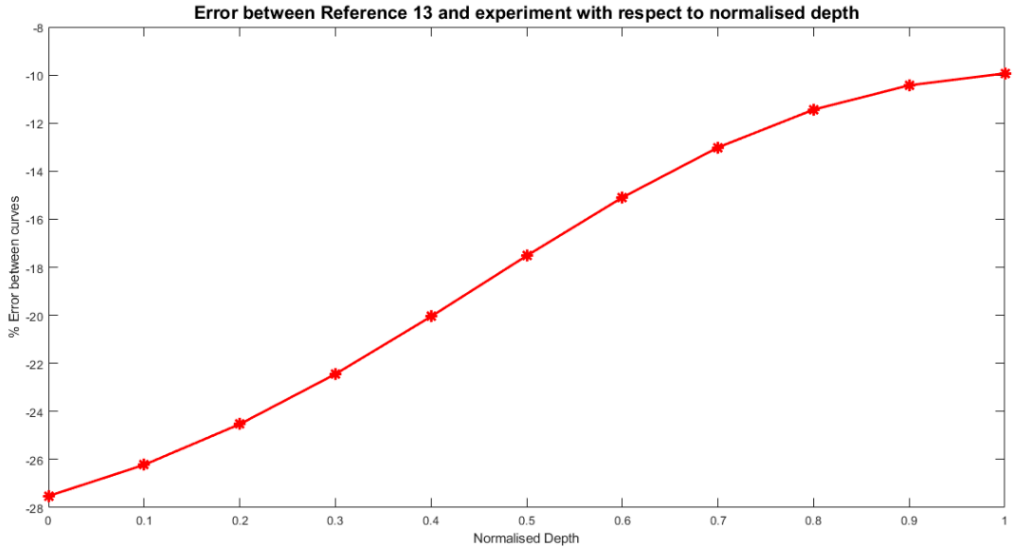

Figure 16. Variation of errors between reference 13 and field experiment corrosion rates with respect to normalised depth.

Despite the normalisation employed, the values were different. This could be explained because of the experiment in the literature happening at deep water from 500 to 5180 m in the Indian Ocean having a tropical climate and with a very different seawater environment and marine colonisers, whereas the experiment carried out the present study was done in temperate shallow water of the North Sea. It is interesting that similar that this trend does exist and would have to be tested with more results from different sites and depths to simulate and check this observation.

A trend though clear, and it could be suggested from the analysis that the array was in the water long enough to reflect that depth influence with respect to seawater.

To the corrosion rate against the depth, a quadratic equation was fitted to develop a mathematical correlation as shown in Figure 17.

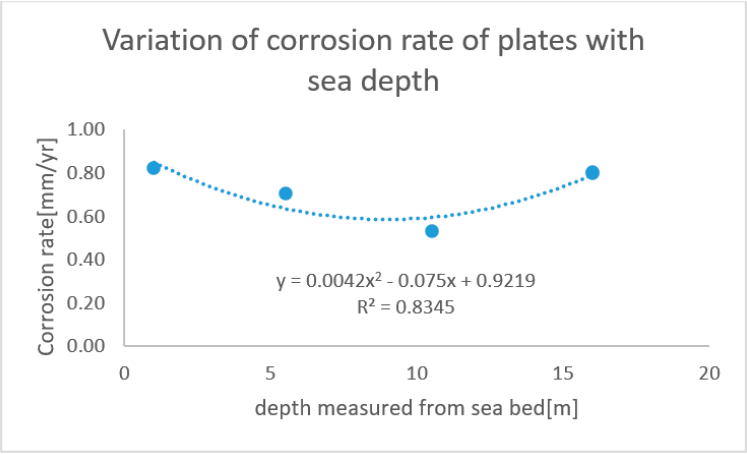

Figure 17. Variation of corrosion rate of plates with sea depth.

Upon interpolation, the splash zone corrosion rate can be found to be more than 1 mm/yr when placed at 20 m.

The graph was normalised in terms of the depth where the maximum normalisation method had been employed represented in Figure 18:

$$\text{Corrosion rate}[\text{mm/yr}] = 1.0754(\text{ND})^2 - 1.2133(\text{ND}) + 0.9281\ . \tag{6}$$

where CR = corrosion rate, ND = normalised depth:

$$\text{ND} = \frac{\text{depth}}{\textit{maximum depth}} \tag{7}$$

The second analysis is to check the corrosion rate according to the standards based on the corrosion rate for corrosion allowance.

The flowing table based on the DNV J101 standard indicate the level of corrosion rate used for design purposes [30].

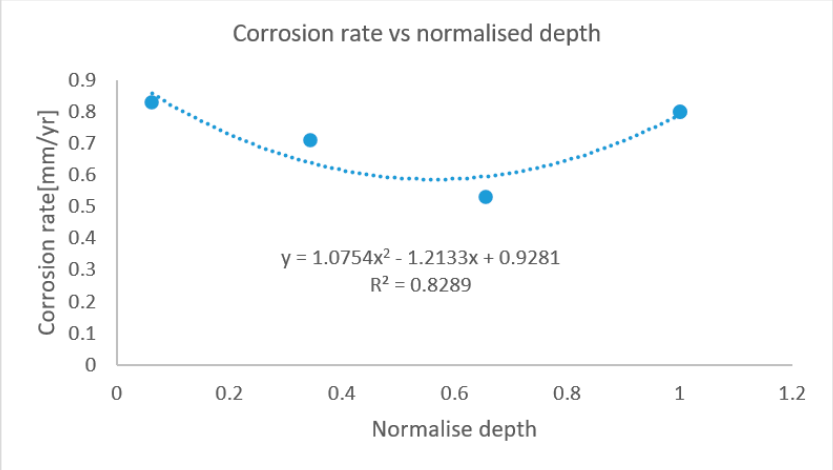

Figure 18. Normalised corrosion depth vs corrosion rates.

The values shown in Table 3 were low when compared to the actual experiment results. From the literature, high corrosion rates were reported from 0.9 and 1.4 mm/year in Alaska and the Gulf of Mexico respectively [31]. An observation on corrosion pits showed the multiplying effect of pit growth with regard to dissolved inorganic nitrogen (DIN) [32]. A good observation regarding the 4-Blue plate which is the closest to the seabed indicate the impact of Nitrogen on the corrosion rates shown in Figure 19.

Table 3. Standard corrosion rates for different sections.

Environmental Zone	Corrosion Rate [mm/yr]
Buried in soil	0.06–0.10
Submerged zone	0.10–0.20
Intermediate Zone	0.05–0.25
Splash Zone	0.20–0.40
Atmospheric Zone	0.050–0.075

A comparison was carried out based from the data from various researchers from more than 40 sites. The corrosion rate observed in the North Sea from the experiment in the 111 days is the highest observed from Table 4.

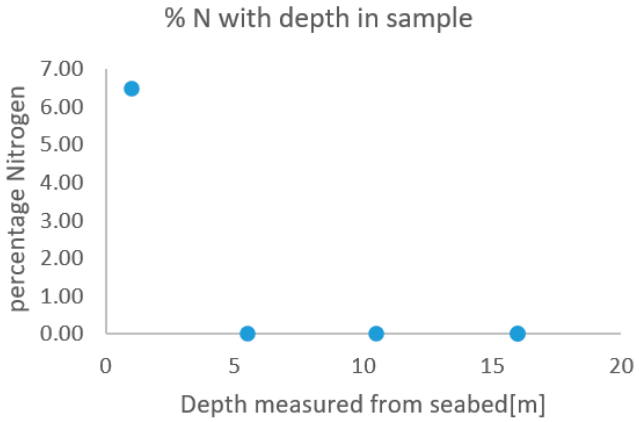

Figure 19. Variation of nitrogen content (%) (in the rust samples colour coded plates) as a function of sea depth).

Some pertinent questions on those corrosion rates provided by the standards would have to be asked. The first one would be when and where were those values obtained from? Which depth or relative sea water depth were the coupons deployed? How long has the exposure been keeping in mind that corrosion is a non-linear process? What were the impacts of the (sulphate reducing bacteria) SRB and other corrosion mechanism? Which grade of steel was it subjected to? Which environment zone and how the annual temperature has changed since the experiment? Has there been any changes to the location over the years with respect to fish farms or other sources of pollutants?

Table 4. Corrosion rates from other research.

Immersed Conditions				
Location	**Country**	**Exposure Period [Years]**	**Corrosion Rate [mm/year]**	**Reference**
Townsville	Australia	2.0	0.240	[25]
Taylor Beach	Australia	2.0	0.205	[25]
Williamstown	Australia	1.5	0.233	[25]
Queenscliff	Australia	2.0	0.225	[25]
Queenscliff	Australia	1.2	0.458	[25]
Hobart	Australia	2.0	0.230	[25]
Hobart	Australia	3.0	0.233	[25]
Port Arthur	Australia	2.1	0.190	[25]
Boston	USA	18.0	0.064	[25]
Norfolk	USA	15.0	0.098	[25]
Key West	USA	22.0	0.075	[25]
Coco Solo	USA	24.0	0.135	[25]
San Diego	USA	18.0	0.100	[25]
Alameda	USA	21.0	0.075	[25]
Puget Sound	USA	9.0	0.086	[25]
Pearl Harbor	USA	2.0	0.360	[25]
Buzzard Bay	USA	5.0	0.020	[25]
LA Costa Island	USA	10.0	0.000	[25]
Kure Beach	USA	5.0	0.000	[25]
Harbor Island	USA	5.0	0.240	[25]
Tokyo Bay	Japan	11.0	0.136	[25]
Yokohama Port	Japan	11.0	0.182	[25]
Trondheim	Norway	26.0	0.092	[25]
Trondheim	Norway	24.0	0.054	[25]

Table 4. *Cont.*

Immersed Conditions				
Location	**Country**	**Exposure Period [Years]**	**Corrosion Rate [mm/year]**	**Reference**
Port Adelaide	Australia	52.0	0.031	[25]
Harbor Island	USA	5.0	0.250	[25]
Newcastle	UK	89.0	0.007	[25]
Thames Estuary	UK	8.0	0.071	[25]
North Sea	UK	7.2	0.154	[25]
Moreton Bay	Australia	2.0	0.230	[25]
Newcastle Harbour	Australia	2.2	0.123	[25]
Taylor Beach	Australia	2.2	0.136	[25]
Coffs Harbour	Australia	2.0	0.150	[25]
Campeche	Mexico		0.280	[23]
New Jersey	USA	0.5	0.213	[27]
		1.0	0.322	[27]
		3.0	0.107	[27]
		5.0	0.100	[27]
North Carolina	USA	0.5	0.165	[27]
		1.0	0.213	[27]
		3.0	0.214	[27]
		5.0	0.224	[27]
Florida	USA	0.5	0.146	[27]
		1.0	0.119	[27]
		3.0	0.124	[27]
		5.0	0.075	[27]
Texas	USA	0.5	0.120	[27]
		1.0	0.105	[27]
		3.0	0.099	[27]
		5.0	0.137	[27]
California	USA	0.5	0.550	[27]
		1.0	0.121	[27]
		2.9	0.173	[27]
		5.0	0.207	[27]
Hawai	USA	0.5	0.240	[27]
		1.0	0.536	[27]
		3.2	0.204	[27]
		5.0	0.097	[27]
Talara	Peru	0.5	0.196	[27]
		1.0	0.147	[27]
		3.1	0.129	[27]
		5.0	0.136	[27]
Sakata Harbor	Japan	0.5	0.089	[27]
		1.0	0.171	[27]
		3.1	0.068	[27]
		5.0	0.094	[27]
Genoa	Italy	0.5	0.194	[27]
		1.0	0.214	[27]
		3.1	0.224	[27]
		5.0	0.115	[27]
Sjaelland	Denmark	0.5	0.106	[27]
		1.0	0.122	[27]
		3.1	0.091	[27]
		5.0	0.100	[27]

Due to complexity of marine corrosion, should the wind farm developers be required to test the environment in corrosion terms to optimise their corrosion allowance and corrosion protection strategies rather than getting the data from the standard? This study denotes such a variation and it is

good to keep in mind the dynamic nature of the oceans and the commercial activities like fish farming and the consequences of those parameters corrosion. This can tend to have wider consequences for instance in terms of corrosion fatigue and the SN curve that was derived from artificial seawater. This might be a gross understatement the fatigue life under real conditions especially if the corrosion rate is as high as observed.

5. Conclusions

The field experiment results can be summarised as:

- A new deployment method has been developed to characterise free corrosion (natural corrosion) to profile the corrosion rate with respect to depth for steel S355, a study that has not been carried out as yet according to the literature.
- The main advantage of using this system is that it reflects the variabilities in the immersed zones without requiring other structures to suspend it to and that water depth does have an influence on the corrosion rate.
- High levels of corrosion rate had been observed that is way above prescribed standards with the highest being at the closest point to the seabed being 0.83 mm/yr. This result though is very similar to the lowest astronomical tide being 0.80 mm/yr. This gave a quadratic function of corrosion rate with respect to tidal depth.
- The highest corrosion rates observed were four times higher than the ones prescribed by the DNV J101-Standards and considerably higher than the field experiments results from 43 other sites.
- Further investigation on the reason behind the trend in corrosion has been done by carrying out the EDS method on the rust particles. Nitrogen at the seabed might have been the reason for the higher corrosion rates.
- After 111 days, the main mechanism of corrosion is still aerobic but traces of sulphur indicate that anaerobic corrosion will happen.
- There were only two arrays recovered out of five and to boost confidence in the results similar experiments will have to be done.
- It is important that the array be strengthened especially for the connection of the lower frame and the anchors by using high strength marine chains rather than ropes to survive the harsh environment of the North Sea.

Author Contributions: Conceptualization, W.K. and P.C.; Data curation, W.K.; Funding acquisition, F.B.; Methodology, W.K. and P.C.; Writing—original draft, W.K.; Writing—review & editing, W.K. and P.C. All authors have read and agreed to the published version of the manuscript.

Funding: This work was supported by grant EP/L016303/1 for Cranfield University, the University of Oxford and Strathclyde University, Centre for Doctoral Training in Renewable Energy Marine Structures (REMS) (http://www.rems-cdt.ac.uk/) from the UK Engineering and Physical Sciences Research Council (EPSRC). This research received no external funding.

Conflicts of Interest: The authors declare no conflict of interest.

Appendix A

Table A1. Raw and processed data from mass loss.

		Mass/g		Mass Loss/g	Mass Loss/g
Label	**Un-Corroded**	**After without Cleaning**	**After with Cleaning**	**Before-After without**	**Before—After with**
1 black	1661.4	1597.6	1588	63.8	73.4
3 black	1666.9	1615.2	1602.4	51.7	64.5
1 blue	1629.9	1582.2	1574.4	47.7	55.5
2 blue	1647.7	1609.1	1599.1	38.6	48.6
4 blue	1661	1594.3	1585.6	66.7	75.4

Appendix B

Table A2. Percentage weight from EDS.

2 Blue	**Percentage Weight**														
Statistics	**N**	**Na**	**Mg**	**Al**	**Si**	**P**	**S**	**Cl**	**K**	**Ca**	**Ti**	**V**	**Cr**	**Mn**	**Fe**
Max	0	2.54	0.44	1.22	2.34	0.28	1.33	4.21	0.43	1.2	0	2.17	1.08	0.54	57.14
Min	0	0.66	0.18	0.24	0.22	0.11	0.45	2.21	0.07	0.07	0	0.11	0.14	0.21	36.55
Average	0	1.4	0.31	0.71	1.09	0	0.79	2.9	0.3	0.46	0	0	0	0	46.86
1 black															
Statistics	N	Na	Mg	Al	Si	P	S	Cl	K	Ca	Ti	V	Cr	Mn	Fe
Max	0	1.39	0.49	0.62	1.12	0	0.57	3.22	0.22	0.32	0	0.28	0.2	0	61.06
Min	0	0.43	0.19	0.3	0.44	0	0.17	0.88	0.07	0.09	0	0.28	0.2	0	40.56
Average	0	0.8	0.33	0.43	0.7	0	0.34	1.86	0.13	0.22	0	0	0	0	52.55
4 blue															
Statistics	N	Na	Mg	Al	Si	P	S	Cl	K	Ca	Ti	V	Cr	Mn	Fe
Max	6.5	2.52	0.81	3.23	5.58	0.63	1.23	3.22	1.08	1.51	0.18	0.67	0.72	0.35	55.83
Min	4.4	1.02	0.12	0.21	0.28	0.06	0.31	1.35	0.07	0.13	0.18	0.15	0.72	0.35	4.58
Average	5.3	1.51	0.52	1.45	2.27	0.21	0.89	2.29	0.55	0.65	0	0	0	0	39.19
3 black															
Statistics	N	Na	Mg	Al	Si	P	S	Cl	K	Ca	Ti	V	Cr	Mn	Fe
Max	0	0.94	0.38	1.63	2.78	0.05	0.66	2.36	0.34	0.23	0.11	0	0	0.5	64.67
Min	0	0.16	0.37	0.1	0.23	0.05	0.25	0.64	0.12	0.07	0.11	0	0	0.5	40.69
Average	0	0.53	0	0.71	1.2	0	0.48	1.6	0.22	0	0	0	0	0	50.34
1 blue															
Statistics	N	Na	Mg	Al	Si	P	S	Cl	K	Ca	Ti	V	Cr	Mn	Fe
Max	0	2.8	1.48	4.31	11.29	0.23	2.04	4.26	1.46	3.2	0.33	0	0.93	0.41	67.36
Min	0	0.54	0.26	0.49	0.46	0.04	0.31	1.34	0.19	2.34	0.33	0	0.28	0.41	14.3
Average	0	1.3	0	1.75	4.77	0	1.09	2.53	0.68	0	0	0	0	0	38.67

References

1. De Rucoba, D.F.; Rodríguez, Á.; Arias, R.R. Degradation and corrosion testing of materials and coating systems for offshore wind turbine substructures in North Sea waters. In Proceedings of the International Wind Engineering Conference, IWEC 2014, Hannover, Germany, 3–4 September 2014. No. SEPTEMBER 2014.
2. Pawsey, C. *The Importance of Corrosion Protection on Offshore Wind Farms*; Corrosion-Offshore: Brazil, 2015.
3. JAhuir-Torres, J.; Simandjuntak, S.; Bausch, N.; Farrar, A.; Webb, S.; Nash, A.; Thomas, B.; Muna, J.; Jonsson, C.; Matthew, D. Corrosion threshold data of metallic materials in various operating environment of offshore wind turbine parts (tower, foundation, and nacelle/gearbox). *Data Brief* **2019**, *25*, 104207. [CrossRef] [PubMed]
4. Mehmanparast, A.; Mehmanparast, A.; Kolios, A. Materials selection for XL wind turbine support structures: A corrosion-fatigue perspective. *Mar. Struct.* **2018**, *61*, 381–397. [CrossRef]
5. Ahuir-Torres, J.I.; Bausch, N.; Farrar, A.; Webb, S.; Simandjuntak, S.; Nash, A.; Thomas, B.; Muna, J.; Jonsson, C.; Mathew, D. Benchmarking parameters for remote electrochemical corrosion detection and monitoring of offshore wind turbine structures. *Wind. Energy* **2019**, *22*, 857–876. [CrossRef]
6. Maher, M. Perforated Offshore Monopile for Corrosion Control and Enhanced Marine Habits. *Mater. Perform.* **2019**. Available online: http://resources.nace.org/pdfs/mp-awards/Florida-Institute-Technology-Perforated-Offshore-Monopile.pdf.
7. Zhou, S.; Zhu, X.; Yan, Q. One-step electrochemical deposition to achieve superhydrophobic cobalt incorporated amorphous carbon-based film with self-cleaning and anti-corrosion. *Surf. Interface Anal.* **2017**, *50*, 290–296. [CrossRef]
8. Momber, A.W. Corrosion and corrosion protection of support structures for offshore wind energy devices (OWEA). *Mater. Corros.* **2010**, *62*, 391–404. [CrossRef]

9. Plagemann, P.; Momber, A. Corrosion Protection of Offshore Wind Energy Constructions in Germany: Challenges and Approaches. *J. Telecommun. Electron. Comput. Eng.* **2018**, *10*, 1–4.
10. Price, S.J.; Figueira, R.B. Corrosion Protection Systems and Fatigue Corrosion in Offshore Wind Structures: Current Status and Future Perspectives. *Coatings* **2017**, *7*, 25. [CrossRef]
11. Ioannou, A.; Angus, A.; Brennan, F. A lifecycle techno-economic model of offshore wind energy for different entry and exit instances. *Appl. Energy* **2018**, *221*, 406–424. [CrossRef]
12. Lioudis, N. How do average costs compare among various oil drilling rigs? *Investopedia* **2020**, *2020*, 1.
13. Mathiesen, T.; Black, A.; Grønvold, F. *Monitoring and Inspection Options for Evaluating Corrosion in Offshore Wind Foundations*; NACE Corrosion: Vancouver, CA, Canada, 2016.
14. Bjørgum, A.; Knudsen, O.Ø. Corrosion protection of offshore wind turbines. In *Wind Power R&D Semin*; SINTEF: Trondheim, Norway, 2010.
15. Hilbert, L.R.; Black, A.R.; Andersen, F.; Mathiesen, T. Inspection and monitoring of corrosion inside monopile foundations for offshore wind turbines. *Eur. Corros. Congr. 2011 EUROCORR* **2011**, *3*, 2187–2201.
16. Hilbert, L.R.; Mathiesen, T.; Black, A.R.; Christensen, C.; Technology, F. Mud zone corrosion in offshore renewable energy structures. In *Eurocorr 2013*; Eurocorr: Portugal, 2013; pp. 1–5.
17. Dong, X.H.; Yuan, T.J.; Ma, R.-H. Corrosion Mechanism on Offshore Wind Turbine Blade in Salt Fog Environment. *Appl. Mech. Mater.* **2013**, *432*, 258–262. [CrossRef]
18. Zhang, J.; Hertelé, S.; De Waele, W. A Non-Linear Model for Corrosion Fatigue Lifetime Based on Continuum Damage Mechanics. *MATEC Web Conf.* **2018**, *165*, 03003. [CrossRef]
19. Buslov, V. Corrosion of Steel Sheet Piles in Port Structures. *J. Waterw. Port Coastal Ocean Eng.* **1983**, *109*, 273–295. [CrossRef]
20. Mith, M.; Bardiau, M.; Brennan, R.; Burgess, H.; Caplin, J.; Ray, S.; Urios, T. Accelerated low water corrosion: The microbial sulfur cycle in microcosm. *Npj Mater. Degrad.* **2019**, *3*, 1–11. [CrossRef]
21. Melchers, R.E.; Jeffrey, R.J. Corrosion of steel piling in seawater harbours. *Proc. Inst. Civ. Eng. Marit. Eng.* **2014**, *167*, 159–172. [CrossRef]
22. Garcia, A.; Valdez-Salas, B.; Schorr, M.; Zlatev, R.; Eliezer, A.; Hadad, J. Assessment of marine and fluvial corrosion of steel and aluminium. *J. Mar. Eng. Technol.* **2010**, *9*, 3–9. [CrossRef]
23. Valdez-Salas, B.; Ramirez, J.; Eliezer, A.; Schorr, M.; Ramos, R.; Salinas, R. Corrosion assessment of infrastructure assets in coastal seas. *J. Mar. Eng. Technol.* **2016**, *15*, 1–11. [CrossRef]
24. Traverso, P.; Canepa, E. A review of studies on corrosion of metals and alloys in deep-sea environment. *Ocean Eng.* **2014**, *87*, 10–15. [CrossRef]
25. Melchers, R.E.; Jeffrey, R. Effect of Immersion Depth on Marine Corrosion of Mild Steel. *Corros. Sci.* **2005**, *61*, 895–906. [CrossRef]
26. Blekkenhorst, F.; Ferrari, G.M.; Van Der Wekken, C.J.; Ijsseling, F.P. Development of high strength low alloy steels for marine applications: Part 1: Results of long term exposure tests on commercially available and experimental steels. *Br. Corros. J.* **1986**, *21*, 163–176. [CrossRef]
27. Kirk, W.; Pikul, S. Seawater Corrosivity Around the World: Results from Three Years of Testing. *Corrosion in Natural Waters* **2009**, 2. [CrossRef]
28. ASTM International. *Standard Practice for Preparing, Cleaning, and Evaluating Corrosion Test*; ASTM International: West Conshohocken, PA, USA, 2017.
29. Knudsen, O.; Bjørgum, A. New coatings for corrosion protection of offshore wind structures. In Proceedings of the Corrosion Protection for Offshore Wind, Dallas, TX, USA, 15–19 March 2015.
30. DNV. *DNV-OS-J101 Design of Offshore Wind Turbine Structures*; Det Norske Veritas: Oslo, Norway, 2014; pp. 212–214.
31. Powell, C.; Michels, H. Review of Splash Zone Corrosion and Biofouling of C70600 Sheathed Steel During 20 Years Exposure. In *Eurocorr 2006*; Eurocorr: Netherlands, 2006; pp. 1–18.
32. Melchers, R.E. Long-term immersion corrosion of steels in seawaters with elevated nutrient concentration. *Corros. Sci.* **2014**, *81*, 110–116. [CrossRef]